Structure–activity relationships for Co- and Fe-promoted vanadium phosphorus oxide catalysts

Sujata Sajip,[a] Jonathan K. Bartley,[b] Andrew Burrows,[a] Maria-Teresa Sananés-Schulz,[c] Alain Tuel,[c] Jean Claude Volta,[c] Christopher J. Kiely*[a] and Graham J. Hutchings*[b]

[a] *Departments of Engineering and Chemistry, University of Liverpool, Liverpool, UK L69 3BX. E-mail: kiely@liv.ac.uk*

[b] *Department of Chemistry, Cardiff University, P.O. Box 912, Cardiff, UK CF10 3TB. E-mail: hutch@cp.ac.uk*

[c] *Institut de Recherches sur la Catalyse, CNRS, 2 Avenue Albert Einstein, 69626 Villeurbanne cedex, France*

Received (in Montpellier, France) 16th October 2000, Accepted 24th November 2000
First published as an Advance Article on the web 19th December 2000

The effect of Co and Fe doping on vanadium phosphate catalysts, prepared by the reaction of V_2O_5 and H_3PO_4 with isobutanol, for the oxidation of *n*-butane to maleic anhydride is described and discussed. At low levels, both Co and Fe dopants significantly enhance the selectivity and the intrinsic activity to maleic anhydride. A combination of powder X-ray diffraction, ^{31}P NMR spin-echo mapping spectroscopy and transmission electron microscopy, together with catalyst test data, is utilised to analyse the origin of the effects of Co doping. Co appears to be essentially insoluble in crystalline $(VO)_2P_2O_7$ and is preferentially distributed in and stabilises an amorphous VPO material. It is suggested that the origin of the promotional effect of Co is associated with its interaction with the disordered VPO phase. The same techniques have been used to analyse the Fe-doped catalyst, but at present it is not possible to be definitive concerning the specific location of the Fe-dopant within the phases present. Previous studies have indicated that Fe can form a solid solution within $(VO)_2P_2O_7$ and therefore it is probable that the Fe may act as an electronic promoter for this phase. The role of Co, however, emphasises the importance of amorphous vanadium phosphate phases in the catalyst system.

Vanadium phosphates are well established as important industrial catalysts for the conversion of *n*-butane to maleic anhydride.[1,2] The catalysts are produced by activating a catalyst precursor compound, $VOHPO_4 \cdot 0.5H_2O$, termed the hemihydrate, in the *n*-butane–air reaction mixture *in situ* in the reactor. The resultant catalyst often consists of a complex mixture of vanadium(IV) and (V) phosphates[1–3] [*i.e.* $(VO)_2P_2O_7$; $VO(PO_3)_2$; α_I-, α_{II}-, δ-, γ-$VOPO_4$]. Detailed *in situ* laser Raman spectroscopy[4] has been used to study this process and, together with *ex situ* transmission electron microscopy and ^{31}P NMR spectroscopy,[5] has provided a detailed analysis of the evolution of catalysts in the absence of promoter compounds. Two topotactic transformation processes have been observed,[5,6] namely, the direct transformation of $VOHPO_4 \cdot 0.5H_2O$ to $(VO)_2P_2O_7$ and the indirect transformation of $VOHPO_4 \cdot 0.5H_2O$ to δ-$VOPO_4$, which subsequently transforms to $(VO)_2P_2O_7$. However, the ^{31}P NMR spectroscopy shows that, in addition to crystalline $(VO)_2P_2O_7$, a disordered V^{4+}–V^{5+} phase is present in the activated catalyst. It is generally considered that the oxidation of *n*-butane to maleic anhydride, a 14-electron process, requires the close proximity of V^{5+} and V^{4+} cations, but the precise nature of the active site is still a matter of much speculation.[1,7] Recently, Coulston *et al.*[8] have shown that the presence of V^{5+} is essential for the formation of maleic anhydride, thereby confirming earlier pulse reaction experiments.[9]

Vanadium phosphate catalysts used industrially typically contain additives[2] (Mo, Co, Fe) to promote the catalytic performance by improving the yield of maleic anhydride and the conversion of *n*-butane. To date, most structural and mechanistic studies of vanadium phosphate catalysts have been restricted to non-promoted formulations. In this paper, we address the structure of the catalyst precursor and activated catalysts for Co- and Fe-doped vanadium phosphate catalysts using a combination of transmission electron microscopy, powder X-ray diffraction and ^{31}P NMR spectroscopy since, as we have shown,[5] this combination of techniques is very potent in characterising VPO catalysts. We have previously shown[10] that addition of low levels of Co and Fe as dopants can influence the balance of V^{5+}–V^{4+} in the catalyst. In this paper, we further explore the effect of Co and Fe promoters on both catalyst performance and micro-structure, in particular to determine whether these promoters can be associated with a specific VPO phase.

Experimental

Catalyst preparation and testing

The undoped precursor was prepared by adding V_2O_5 (11.8 g) to isobutanol (250 ml). H_3PO_4 (16.49 g, 85%) was then introduced and the mixture was refluxed for 16 h. Doped catalysts (in the range 1 to 5 at% dopant) were prepared by adding the required amount of cobalt or iron acetyl acetonate to the initial reaction mixture. After refluxing, the solid was recovered by filtration and washed with isobutanol (200 ml) and ethanol (150 ml, 100%). The resulting solid was refluxed in water (9 ml g^{-1} solid), filtered hot and dried in air (110 °C, 16 h).

The catalyst precursor was loaded in a fixed bed laboratory microreactor[5] and activated by heating to 430 °C in the reaction mixture (*n*-butane–oxygen–helium, 1.6 : 1.8 : 80.4) at a

volume hourly space velocity of 1000 ml gas (ml catalyst)$^{-1}$ h^{-1} and stabilised prior to testing under a variety of experimental conditions. The catalyst performance was monitored using on-line gas chromatography.

Catalyst characterisation

Powder X-ray diffraction was carried out using a Siemens D 500 diffractometer operating with a Cu-Kα source. BET surface area measurements were carried out using nitrogen adsorption at liquid nitrogen temperatures.

Samples suitable for transmission electron microscopy analysis were prepared by dispersing the catalyst powder onto a lacey carbon film supported on a copper mesh grid. TEM and HREM observations were made in a JEOL 2000EX high-resolution electron microscope operating at 200 kV. This instrument had been fitted with a low-light-level TV camera and a frame-averaging system to allow us to use very low illumination conditions. This latter condition is essential for studying these beam-sensitive vanadium phosphorus oxide compounds. Energy dispersive X-ray (EDX) analysis characterisation was carried out in a JEOL 2000 FR TEM equipped with a LINK system EDS spectrometer.

The ^{31}P NMR measurements were performed on a Bruker MSL 300 NMR spectrometer. The ^{31}P spin-echo mapping method has been shown by Li *et al.*[11] to be a very powerful technique for evaluating the relative proportions of V^{5+} and V^{4+} ions surrounding the P atoms in vanadium phosphate compounds. The ^{31}P NMR spin-echo spectra were recorded under static conditions, using a $90°x–\tau–180°y–\tau$ acquire sequence. The 90° pulse duration was 4.2 μs and τ was 20 μs. For each sample, the irradiation frequency was varied in increments of 100 kHz above and below the ^{31}P resonance of H_3PO_4. The number of spectra recorded was dictated by the frequency limits beyond which no spectral intensity was detectable. The ^{31}P NMR spin-echo mapping information was then obtained by superposition of all the spectra.

Results and discussion

Characterisation of the doped hemihydrate phase

The powder X-ray diffraction patterns of the fresh hemihydrate precursors are shown in Fig. 1. All of the reflections can be indexed to the hemihydrate phase, $VOHPO_4 \cdot 0.5H_2O$ for the doped and undoped materials. In the case of the Co-doped samples, the addition of Co leads to a slight variation in the $[001]^{hemi}/[220]^{hemi}$ relative intensity ratio (undoped VPO 2.6; VPO Co1, 1.9; VPO Co5, 1.3). The effect is much more pronounced for the Fe-doped precursors with the $[001]^{hemi}/[220]^{hemi}$ relative intensity values being 0.84 and 0.42 for the 1 and 5 at% Fe-doped samples, respectively. Furthermore, for the 5 at% Fe-doped sample, there is a significant broadening of the $[001]^{hemi}$ reflection when compared with the undoped hemihydrate. Indeed, the powder X-ray diffraction pattern of the 5 at% Fe-doped hemihydrate is similar to that for a hemihydrate prepared by reaction of $VOPO_4 \cdot 2H_2O$ with a primary alcohol.[12] It is possible that the Fe dopant may be playing a similar role to alcohols, which can be occluded within the hemihydrate layer structure. For the 5 at% Co- and 5 at% Fe-doped hemihydrates, an additional reflection at $d = 6.4$ and 6.6 Å, respectively, is observed. This cannot be indexed to any known VPO compound and may be due to mixed M–VPO hydrated phases, where M = Co or Fe. For the 5 at% Fe-doped hemihydrate, there is an additional weak reflection at $d = 7.4$ Å, corresponding to the [001] reflection of $VOPO_4 \cdot 2H_2O$. This indicates that a small amount of oxidation has occurred due to Fe-doping, and this effect was also noted in an earlier study of Fe-doped hemihydrate prepared using aqueous HCl as reducing agent.[13]

The ^{31}P NMR spin-echo mapping spectra of the doped

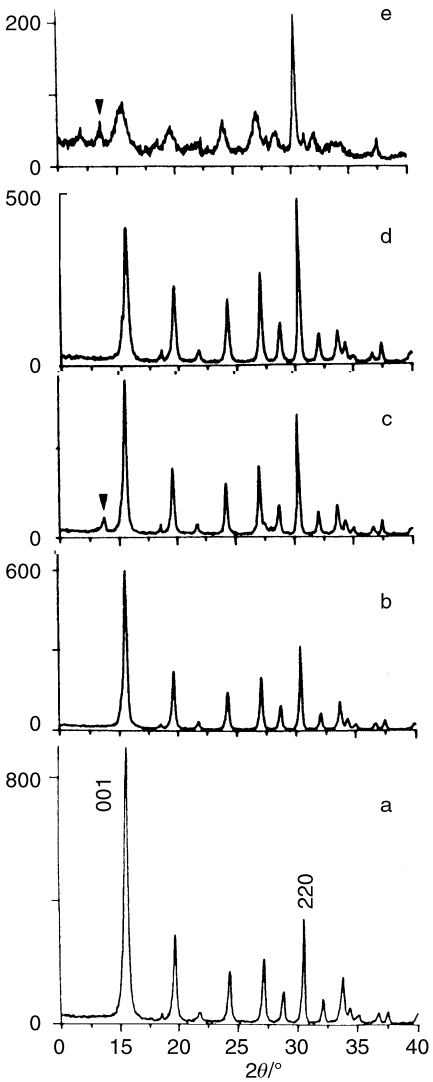

Fig. 1 Powder X-ray diffraction patterns of hemihydrates: (a) VPO, (b) VPO Co1, (c) VPO Co5, (d) VPO Fe1, (e) VPO Fe5.

hemihydrates are shown in Fig. 2. All show a signal at 1625 ppm, which is assigned to P atoms coordinated by V^{4+} cations in the hemihydrate.[14] A weaker signal at 0 ppm is also observed, which is attributed to P atoms coordinated to V^{5+} cations. This also indicates the presence of a $VOPO_4$ phase in the precursor.

Electron microscopy of the hemihydrate precursors showed that all the doped samples have a similar characteristic rhomboidal plate-like morphology. For the undoped hemihydrate, the dimensions of the rhomboid platelet were typically about 2 μm × 1 μm with a platelet thickness of typically 0.03–0.1 μm. Doping with Co and Fe did not significantly change the morphology (Fig. 3) except that the platelet dimensions increased to typically 3 μm × 2 μm. Selected area diffraction patterns indicated that the major and minor axes of the rhomboid correspond to the [100] and [010] directions of the $VOHPO_4 \cdot 0.5H_2O$ crystal structure, respectively. Chemical analysis using energy dispersive X-ray analysis indicated that the Fe and Co were homogeneously dispersed throughout the hemihydrate crystal. However, in the case of the 5 at% Co-doped sample, some regions of high Co concentration were noted and these are considered to be due to the formation of cobalt phosphate as a separate phase, which was confirmed from selected area diffraction patterns of selected crystals.

Catalytic performance measurements

Catalytic performance data following activation *in situ* in the reactor in flowing *n*-butane–oxygen–helium catalysts are

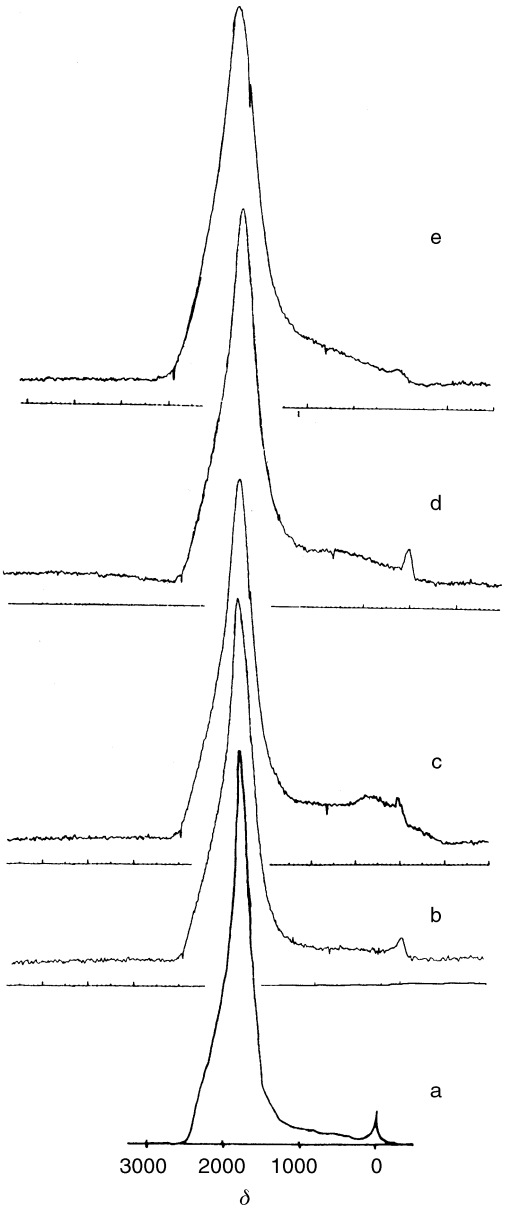

Fig. 2 ^{31}P NMR spin-echo mapping spectra of hemihydrates: (a) VPO, (b) VPO Co1, (c) VPO Co5, (d) VPO Fe1, (e) VPO Fe5.

shown in Table 1. Addition of Co at the 1 at% and 5 at% levels increased the selectivity to maleic anhydride at high *n*-butane conversions and also increases the intrinsic activity. A similar effect is noted for the addition of Fe. The enhancement in intrinsic activity, which is observed at both 400 and 430 °C, as well as at two reactant flow rates, can be considered a general feature for the addition of Fe and Co to this vanadium phosphate catalyst. The effects are most pronounced at the 1% doping level and increasing the level of the dopant decreases the promotion effect. This behaviour is similar to that observed in previous studies of promoter concentration on catalyst performance for catalysts prepared using aqueous HCl as a reducing agent.[2] Of the two promoters investigated, Co gives the greatest enhancement in intrinsic activity. Of particular importance is the observation that the addition of Co and Fe increases the selectivity to maleic anhydride at moderate butane conversions (*i.e.* S_{25}^{MA}, Table 1). This effect is significant and contributes to the promotional effect.

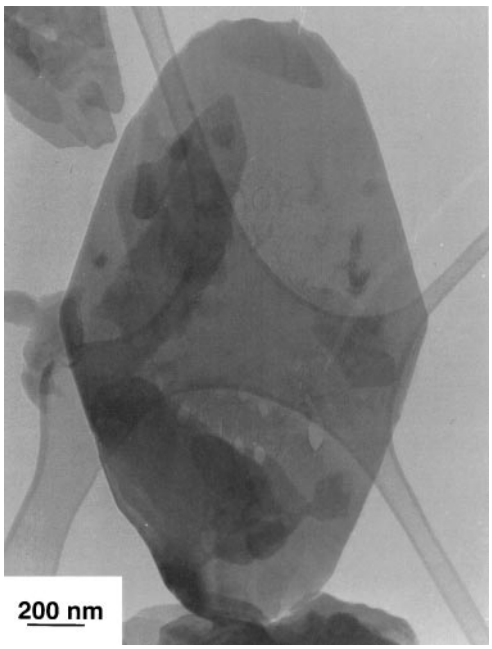

Fig. 3 Bright field transmission electron micrograph and selected area diffraction pattern for VPO Co1 hemihydrates.

Characterisation of the doped VPO activated catalysts

Powder X-ray diffraction patterns of the activated catalysts are shown in Fig. 4). The materials can all be classed as poorly crystalline, although the diffraction patterns for the 1% doped samples are a little sharper. A comparison of the diffraction patterns with those obtained from crystalline standards of $(VO)_2P_2O_7$ and the various $VOPO_4$ phases[15] does clearly show the presence of $(VO)_2P_2O_7$ in all the samples as characterised by the 200, 024 and 032 reflections at 23, 28.45 and 29.94°, respectively.

Co-doped catalysts. The ^{31}P NMR spin–echo mapping spectra of the Co-doped activated catalysts are shown in Fig.

Table 1 Catalyst performance data[a]

Catalyst	Surface area/m^2 g^{-1}					Intrinsic activity[e] /10^{-5} mol MA m^{-2} h^{-1}		
	Precursor	Activated catalyst	$S_0^{MA\,b}$ (%)	$S_{25}^{MA\,c}$ (%)	$C^{but\,d}$ (%)	430 °C 1000 h^{-1}	400 °C 1000 h^{-1}	400 °C 2000 h^{-1}
VPO	11	13	80.0	50.3	16	1.94	1.20	0.98
VPO Col	9	16	74.5	71.4	36	3.52	3.03	1.92
VPO Co5	6	10	85.5	62.4	16	2.51	1.82	1.18
VPO Fe1	7	19	74.5	73.5	41	2.44	2.29	1.82
VPO Fe5	7	14	70.5	72.0	38	1.79	1.58	1.24

[a] Following activation in C_4H_{10}–O_2–He = 1.6 : 18 : 80.4 at 1000 ml gas (ml catalyst)$^{-1}$ h for *ca.* 72 h. [b] Selectivity to maleic anhydride extrapolated to zero *n*-butane conversion at 400 °C. [c] Selectivity to maleic anhydride at 25% *n*-butane conversion at 400 °C. [d] *n*-Butane conversion at 400 °C and 2000 ml gas (ml catalyst)$^{-1}$ h^{-1}. [e] Intrinsic activity is defined as mol maleic anhydride synthesised per unit area of catalyst per unit time. Data are given for three sets of reaction conditions: reaction temperature: 430 or 400 °C; gas hourly space velocity: 1000 or 2000 h^{-1}.

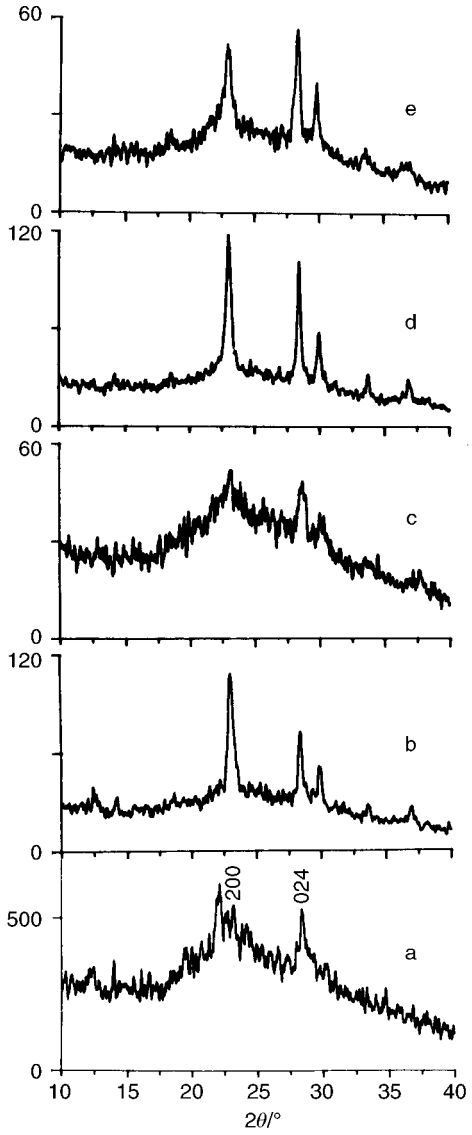

Fig. 4 Powder X-ray diffraction patterns of the activated catalysts: (a) VPO, (b) VPO Co1, (c) VPO Co5, (d) VPO Fe1, (e) VPO Fe5.

5). The spectra all show three signals, at 0 (P associated with V^{5+}), 2400 [characteristic of well crystallized $(VO)_2P_2O_7$] and 200–1500 (characteristic of poorly crystalline/disordered C^{4+}–V^{5+} material) ppm. From a comparison of the undoped and Co-doped activated catalyst, it is apparent that the 1% Co-doped material has a high proportion of well crystallized $(VO)_2P_2O_7$ but it also has a high proportion of the signal associated with the poorly crystalline/disordered material.

Low magnification transition electron micrographs of typical crystallites from VPO and VPO Co1 are shown in Fig. 6. It is clear that the rhomboid platelet morphology of the hemihydrate is retained in these specimens. The undoped VPO catalyst comprises mainly microcrystallites of $(VO)_2P_2O_7$, together with a very small amount of disordered material, and the microscopy of this sample has been described in detail previously.[5] The VPO Co1 platelet is largely disordered material with some $(VO)_2P_2O_7$ crystallites (30–150 nm in size) that preferentially nucleate at the periphery of the platelet, as shown in Fig. 7. In this image, crossed fringes with an interplane spacing of 3.1 Å and an interplanar angle of 81° (corresponding to $[024]^{pyro}$ planes) are resolved, and these are characteristic of the [100] projection of $(VO)_2P_2O_7$. It is clear that doping with 1% Co significantly enhances the proportion of disordered material present in the activated catalysts. Chemical analysis, using energy dispersive X-ray analysis, of the disordered material and an isolated

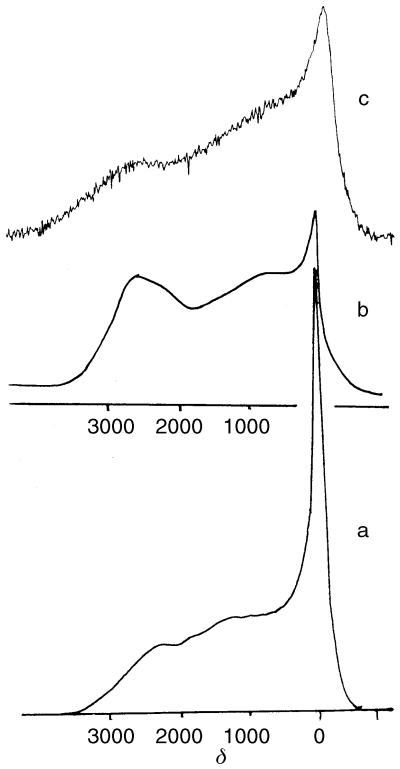

Fig. 5 ^{31}P NMR spin-echo mapping spectra of activated catalysts: (a) VPO, (b) VPO Co1, (c) VPO Co5.

$(VO)_2P_2O_7$ crystallite are shown in Fig. 8. It is clear that, within the limit of detection of 0.1% Co, the $(VO)_2P_2O_7$ crystallites do not contain Co, and the Co dopant is preferentially segregated and exists within the disordered material.

The major morphology present in the VPO Co5 activated catalyst is a very similar platelet morphology to that of VPO Co1. Again, selected area diffraction patterns show reflections due to $(VO)_2P_2O_7$, together with additional reflections due to non-transformed hemihydrate. It is apparent, at this level of doping, that Co is still inhibiting the transformation of the hemihydrate under the reaction conditions. However, an additional phase is present in the VPO Co5 activated catalyst (Fig. 9) but as a very minor component (<1 vol%). Electron diffraction studies indicate that the latter material is disordered. EDX microanalysis of the material contained significantly more Co than the partially transformed $VOHPO_4 \cdot 0.5 H_2O/(VO)_2P_2O_7$ platelets previously described, and it is most likely that the material is cobalt phosphate.

Fe-doped catalysts. The ^{31}P NMR spin-echo mapping spectra for the Fe-doped activated catalysts are shown in Fig. 10. The spectra for VPO Fe1 and VPO Fe5 are very similar and show three signals, at 0, 200–1500 and 2400 ppm, as observed with the Co-doped samples. Qualitative comparison of the spectra indicates that Fe-doping appears to have increased the relative proportions of the signals associated with crystalline $(VO)_2P_2O_7$ and disordered V^{4+}–V^{5+}.

Low magnification transmission electron micrographs of typical crystallites from VPO Fe1 and VPO Fe5 are shown in Fig. 11. It is clear that the rhomboid morphology of the hemihydrate precursor is retained. The platelet interior of the VPO Fe1 material is disordered and it is observed that crystallites of $(VO)_2P_2O_7$ have formed at the edge of the rhomboid platelet; these $(VO)_2P_2O_7$ crystals are *ca.* 40 nm in thickness. In addition to $(VO)_2P_2O_7$, a small amount (3–4 vol%) of α_{II}-$VOPO_4$, as detected by selected area diffraction, was observed to be present. Chemical analysis using energy dispersive X-ray analysis showed that the Fe was uniformly distributed

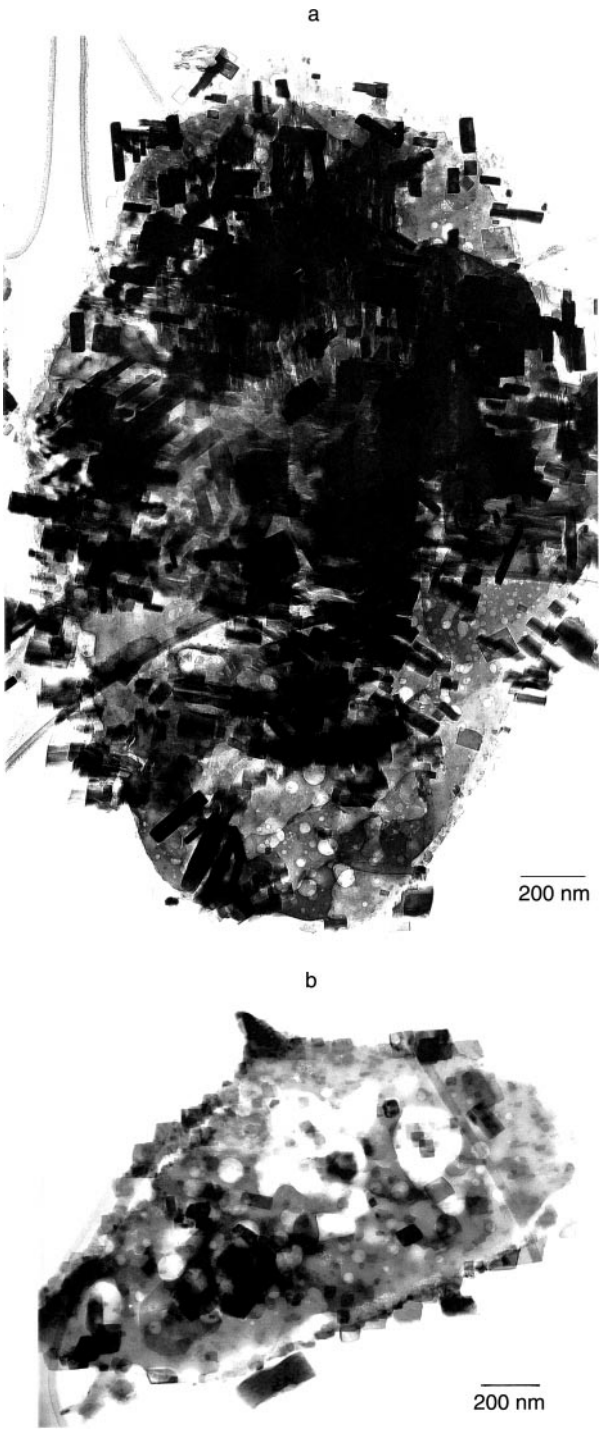

Fig. 6 Bright field transmission electron micrographs of activated catalysts: (a) VPO, (b) VPO Co1.

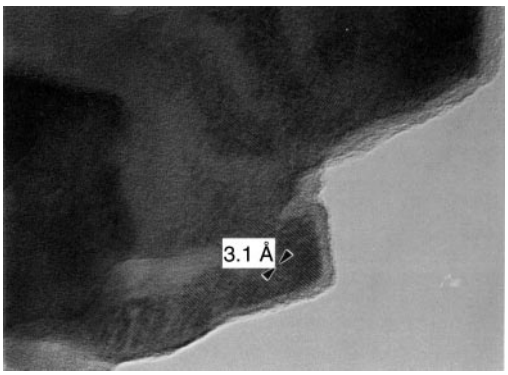

Fig. 7 Bright field transmission electron micrographs of $(VO)_2P_2O_7$ crystallite that has nucleated at the platelet periphery.

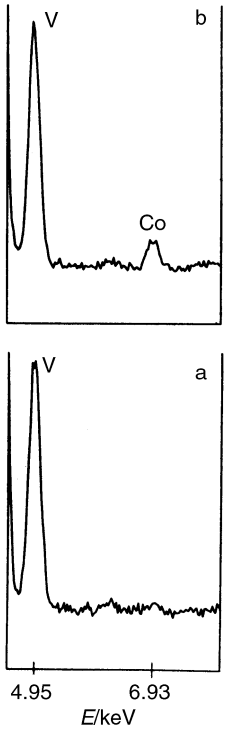

Fig. 8 Energy dispersive X-ray spectra for VPO Co1: (a) $(VO)_2P_2O_7$ crystallite, (b) disordered platelet interior.

throughout the rhomboidal platelet, but at such low levels the chemical analysis of Fe is inevitably inconclusive, because of the possible fluorescence effect from the microscope pole pieces. In view of this, it is not possible to comment further on the distribution of Fe within this material.

For VPO Fe5, the sample comprises rhomboid platelets in which crystallites have nucleated, preferentially at the platelet edges. High resolution imaging and selected area diffraction patterns confirmed these crystallites to be $(VO)_2P_2O_7$. In addition, α_{II}-$VOPO_4$ is present in this sample (10–20 vol%).

Comments on the promotional effects of Fe and Co dopants

It is clear that addition of low levels of Co and Fe to $VOHPO_4 \cdot 0.5H_2O$, prepared by the reaction of V_2O_5 and H_3PO_4 with isobutanol, leads to an improvement in the catalytic performance of the activated material. Both lead to an enhancement in maleic anhydride selectivity and *n*-butane conversion and, in particular, the intrinsic activity. The detailed structural study of the activated catalysts using trans-

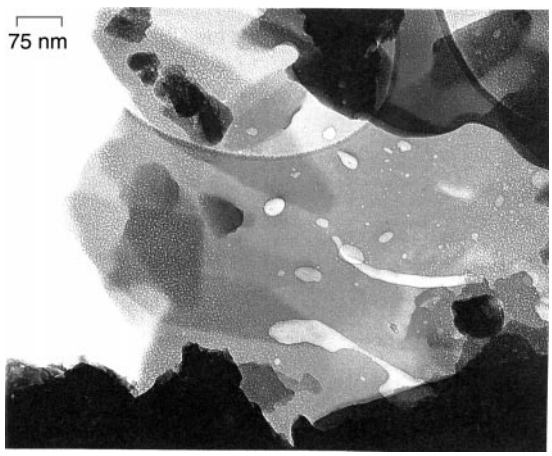

Fig. 9 Bright field transmission electron micrograph of the minor secondary phase observed in VPO Co5.

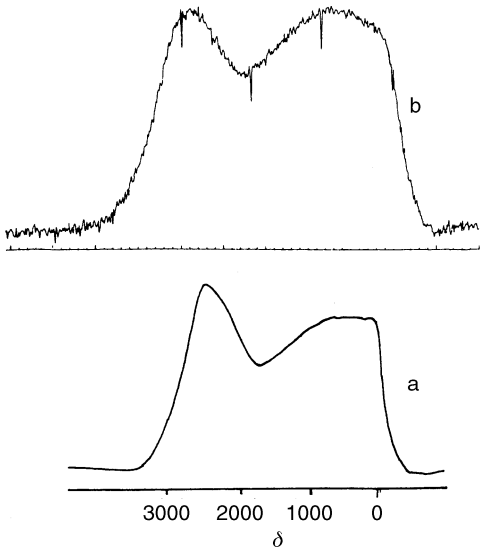

Fig. 10 ^{31}P NMR spin-echo mapping spectra of activated catalysts: (a) VPO Fe1, (b) VPO Fe5.

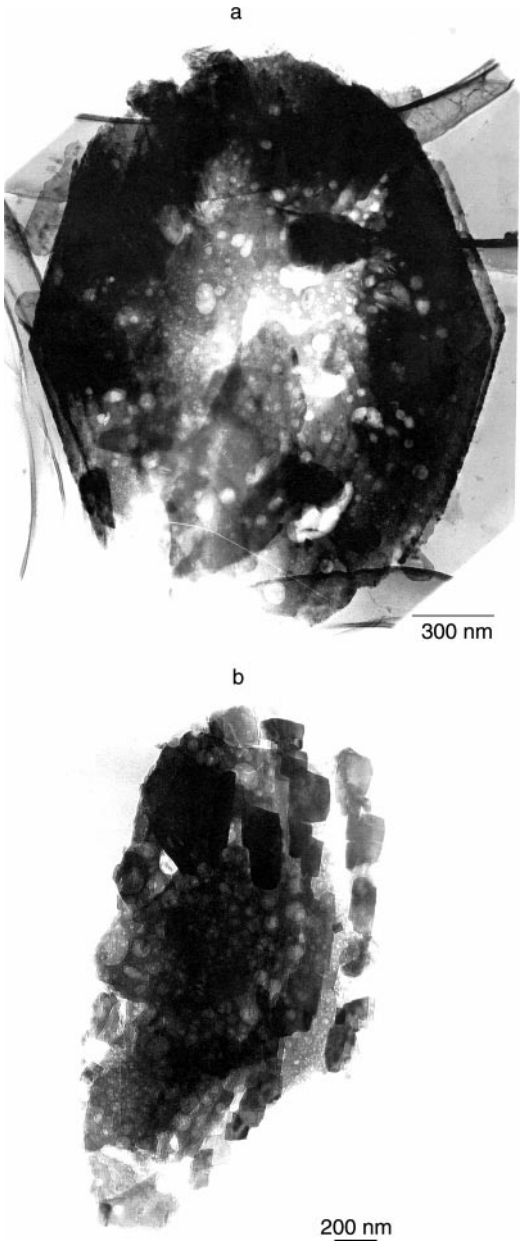

Fig. 11 Bright field transmission electron micrographs of activated catalysts: (a) VPO Fe1, (b) VPO Fe5.

mission electron spectroscopy allows us to comment on the role of Co as a promoter. The Co dopant is effectively insoluble in the $(VO)_2P_2O_7$ crystallites. Although Co is homogeneously dissolved within the initial $VOHPO_4 \cdot 0.5H_2O$, on activation phase separation takes place and the Co preferentially remains in the disordered V^{4+}–V^{5+} material. In addition, the presence of Co appears to stabilise the disordered material and the VPO Co1 sample contains a significant proportion of the disordered material when compared with the equivalent undoped catalyst.[5] Since the addition of 1% Co markedly increases the intrinsic activity and maleic anhydride selectivity, we do not consider that this is due to an increased activity of the crystalline $(VO)_2P_2O_7$ component of the catalyst, since the crystalline $(VO)_2P_2O_7$ is essentially undoped and must retain the catalytic performance of the undoped material. We propose therefore that the Co dopant is acting as a promoter for the disordered VPO material and this provides an indication that disordered VPO phases may be of significance for the oxidation of *n*-butane to maleic anhydride. This is in agreement with a number of previous observations concerning the role of disordered material in vanadium phosphate catalysts.[16] As chemical analysis using EDX is inconclusive for the Fe doped material, it is not possible to comment in detail on the origin of the promotional effect observed with Fe. However, previous studies by Otake[17] have shown that Fe can be present as a solid solution in $(VO)_2P_2O_7$ and a distinct increase in the intrinsic activity for maleic anhydride formation was observed for such $(VO)_{2-x}Fe_xP_2O_7$ solid solutions. In this case, Fe could act as an electronic promoter specifically for $(VO)_2P_2O_7$, probably enabling the re-oxidation of the catalyst or aiding oxygen mobility. It is also possible that Fe is associated with the disordered phase and could act in a similar manner with this material. Hence, the promotional effect observed with Fe may originate from a combination of two effects.

Acknowledgements

We thank the EPSRC and EU (European Human Capital and Mobility Program Contract CHRX-CT92-0065) for financial support.

References

1 *Forum on Vanadyl Pyrophphate Catalyst*, ed. G. Centi, *Catal. Today*, 1994, **16**.
2 G. J. Hutchings, *Appl. Catal.*, 1991, **72**, 1.
3 J. W. Johnson, D. C. Johnston, A. J. Jacobson and J. F. Brody, *J. Am. Chem. Soc.*, 1984, **106**, 8123.
4 G. J. Hutchings, A. Desmartin-Chomel, R. Olier and J. C. Volta, *Nature* (*London*), 1994, **368**, 41.
5 C. J. Kiely, A. Burrows, G. J. Hutchings, K. E. Bere, J. C. Volta, A. Tuel and M. Abon, *Faraday Discuss.*, 1996, **105**, 103.
6 M. Abon, K. E. Bere, A. Tuel and P. Delichere, *J. Catal.*, 1995, **156**, 28.
7 P. L. Gai and K. Kourtakis, *Science*, 1995, **267**, 661.
8 G. W. Coulston, S. R. Bare, H. Kung, K. Birkeland, G. K. Bethke, R. Harlow, N. Herron and P. L. Lee, *Science*, 1997, **275**, 191.
9 J. T. Gleaves, J. R. Ebner and T. C. Kuechler, *Catal. Rev. Sci. Eng.*, 1988, **30**, 49.
10 M. T. Sananés-Schulz, F. B. Abdelouhab, G. J. Hutchings and J. C. Volta, *J. Catal.*, 1996, **163**, 346.
11 J. Li, M. E. Lashier, G. L. Schrader and B. C. Gerstein, *Appl. Catal.*, 1988, **38**, 83.
12 I. J. Ellison, G. J. Hutchings, M. T. Sananés and J. C. Volta, *J. Chem. Soc., Chem. Commun.*, 1994, 1093.
13 G. J. Hutchings, I. J. Ellison, M. T. Sananés and J. C. Volta, *Catal. Lett.*, 1996, **38**, 231.
14 M. T. Sananés, A. Tuel and J. C. Volta, *J. Catal.*, 1994, **145**, 251.
15 F. Benabdelouahab, R. Olier, N. Guilhaume, F. Lefevre and J. C. Volta, *J. Catal.*, 1992, **134**, 151.
16 A. Bruckner, A. Martin, B. Kubias and B. Lucke, *J. Chem. Soc., Faraday Trans.*, 1998, **94**, 2221.
17 M. Otake, US Pat. 1399560, 1975.